

# Selective Sensing of Catechol Aldehydes Levels in Living Systems using FLIM-FRET

John M. Talbott,<sup>‡a</sup> Rachel Wills,<sup>‡a</sup> Rajendra Shirke,<sup>‡a</sup> Leslie Hassanein,<sup>b</sup> David Weinschenker,<sup>b</sup> and Monika Raj<sup>\*a</sup>

<sup>a</sup>Department of Chemistry, Emory University, Atlanta, GA, 30322, USA.

<sup>b</sup>Department of Human Genetics, Emory University School of Medicine, Atlanta, GA, 30322, USA.

<sup>‡</sup> These authors contributed equally

## Abstract

Endogenous catechol aldehydes (CAs), namely 3,4-dihydroxyphenylacetaldehyde (DOPAL) and 3,4-dihydroxyphenylglycolaldehyde (DOPEGAL), play pivotal roles in neurobehavioral, cardiovascular, and metabolic processes. Dysregulation of CA levels contributes to neurological disorders and heart diseases. Thus, detecting imbalances in CAs levels is crucial for diagnosing early stages of CA-associated diseases. Here, we present innovative fluorescent sensors designed for rapid and selective detection of CAs within cells and tissue, overcoming the limitations of conventional diagnostic methods that necessitate cell destruction. The sensor operates by a dual-reaction trigger, leveraging the exceptional selectivity of *o*-phenylenediamine for aldehyde and phenylboronic acid for catechol, resulting in the production of a FRET signal exclusively for CAs in the presence of other aldehydes and catechols within cells. To circumvent issues such as spectral cross-talk, excitation intensity fluctuations, inner filtering, photobleaching, and detector sensitivity, we employed Fluorescence Lifetime Imaging Microscopy (FLIM) combined with FRET (FLIM-FRET) to accurately measure CAs levels at a nanosecond scale. This makes FLIM-FRET highly proficient for live cell and tissue imaging. Remarkably, we utilized this dual-reaction trigger FLIM-FRET system to detect endogenous CAs levels within cells in response to enzyme activators and inhibitors and within diseased-model mice tissue. These probes have the potential to serve as early warning systems for neurological diseases linked to CAs within living systems, laying the foundation for further investigations.

## Introduction

Oxidative deamination of norepinephrine (NE) and dopamine (DA) by monoamine oxidase (MAO) generates catecholaldehydes, namely 3,4-dihydroxyphenylglycolaldehyde (DOPEGAL) and 3,4-dihydroxyphenylacetaldehyde (DOPAL), along with H<sub>2</sub>O<sub>2</sub>.<sup>1-3</sup> Under physiological conditions, these metabolites are primarily detoxified by aldehyde dehydrogenase (ALDH) or aldose reductase (AR) to their corresponding carboxylic acid (DOPAC) or alcohol (DHPG), respectively.<sup>4-5</sup> However, during oxidative stress, there is a dysregulation in catecholamine metabolism, diminishing ALDH and other detoxifying enzyme activity (Figure 1).<sup>6-7</sup> This imbalance leads to an increase in DOPAL and DOPEGAL production and accumulation, which can react with proteins, causing structural and functional alterations.<sup>8-10</sup> Both DOPAL and DOPEGAL are more cytotoxic than their parent catecholamines due to their unique chemical properties, resulting in the formation of stable adducts with proteins and crosslinking with biological molecules.<sup>11</sup> The reactivity of three key components within catechol aldehydes (CAs)—aldehyde, catechol, and alpha

hydroxyl groups, exclusive in DOPEGAL—plays a pivotal role in modifying proteins and fostering crosslinking processes.<sup>12</sup> These alterations include the formation of Schiff bases and thiazolidines with lysine and cysteine, respectively, by the aldehyde group.<sup>13-14</sup> Additionally, under conditions of oxidative stress, the catechol group undergoes transformation into quinones, which subsequently modify lysine and cysteine through Michael-type addition reactions<sup>15</sup> Furthermore, the alpha hydroxy aldehyde moiety of DOPEGAL triggers the generation of Amadori rearrangement products upon reacting with lysine and the N-terminus.<sup>16</sup>

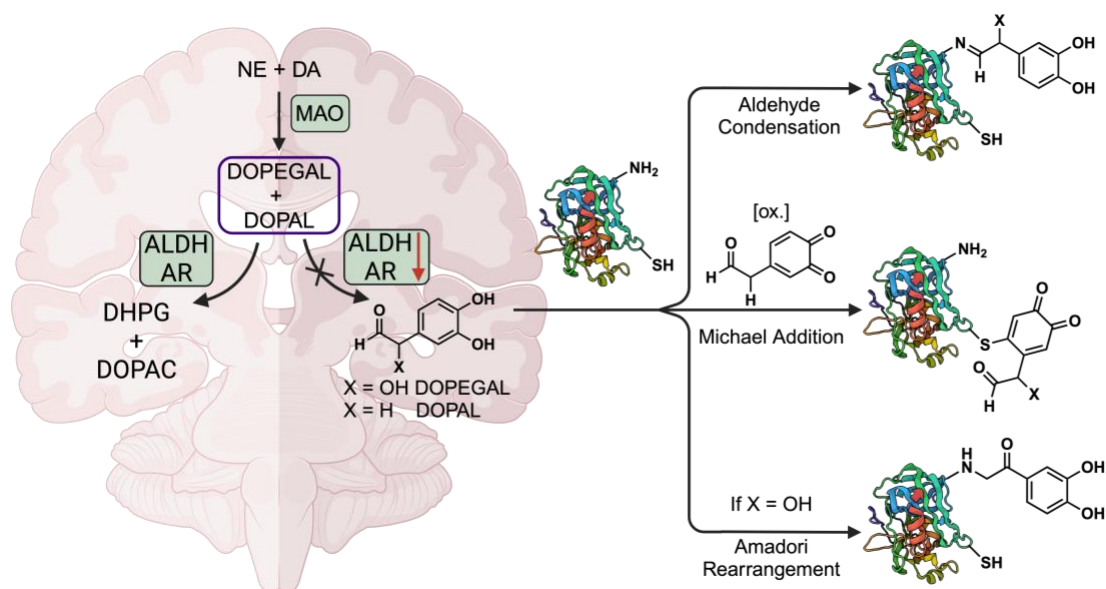


**Figure 1:** Metabolic pathway of norepinephrine (NE) and dopamine (DA) conversion to DOPEGAL and DOPAL by Monoamine oxidase (MAO) which are processed by aldehyde dehydrogenase (ALDH) and aldehyde reductase (AR) to non-toxic dihydroxyphenylglycol (DHPG) and 3,4-Dihydroxyphenylacetic acid (DOPAC). Dysregulation of ALDH and AR leads to accumulation of DOPEGAL and DOPAL, which can form covalent crosslinks with biological nucleophiles leading the diseased states.

These reactions permanently alter protein structures and functions, contributing to various neurodegenerative diseases including, Parkinson’s disease (PD), Alzheimer’s disease (AD), schizophrenia, and Huntington’s disease,<sup>17-21</sup> and cardiac injuries from ischemia, diabetes, and hypertension.<sup>22-25</sup> Therefore, Identifying and quantifying catechol aldehydes is crucial for the early detection of neurological and cardiovascular disorders. However, traditional detection methods such as high-pressure liquid chromatography (HPLC),<sup>26</sup> mass spectroscopy (MS),<sup>27</sup> microdialysis,<sup>28</sup> capillary electrophoresis (CE),<sup>29</sup> electrochemical analysis,<sup>30</sup> and optical spectroscopy<sup>31</sup> are time-consuming, lack selectivity, require large sample volumes, and are not optimal for efficient detection.<sup>32</sup> Moreover, these techniques necessitate cell destruction, leading to inaccuracies due to oxidative stress-related artifacts.<sup>33-34</sup> Additionally, cell destruction fails to capture cell-to-cell variability in CA levels, resulting in the loss of spatiotemporal information and the inability to track CA fluctuations in real-time within live cells. Another approach to assess CA cytotoxicity involves identifying protein crosslinks, but this method does not offer early warning signals as the neurodegenerative process is typically advanced by the time crosslinking occurs.<sup>5,35-38</sup>

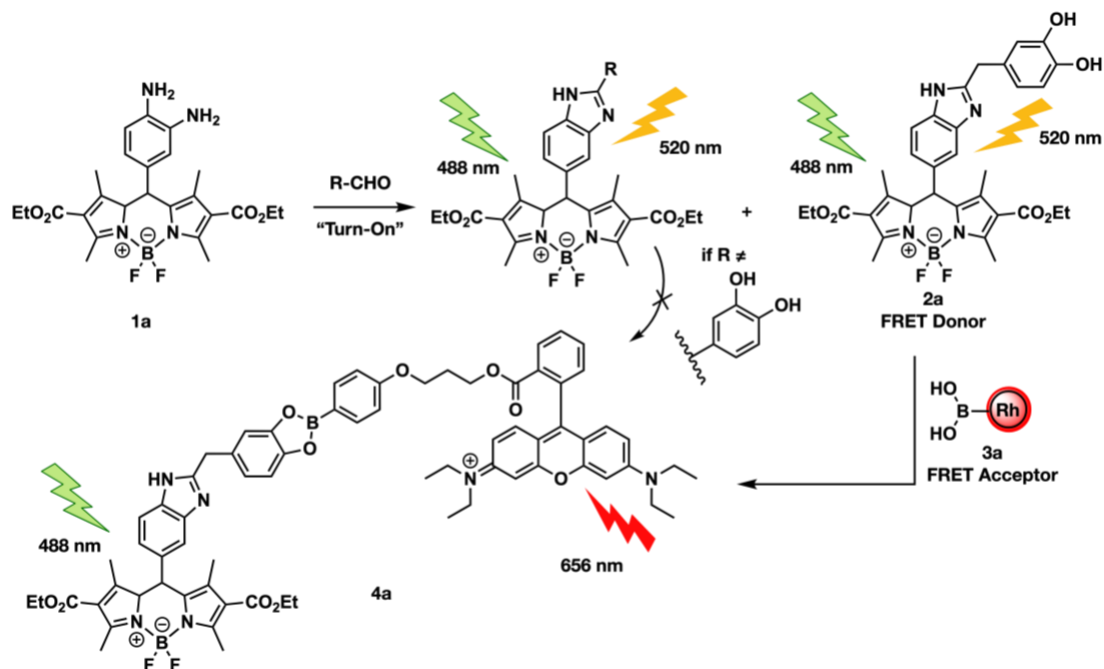


**Figure 2.** “Turn-On” fluorescence of probe **1a** with aldehydes and selective FRET formation of catechol benzimidazole FRET donor **2a** and boronic acid FRET acceptor **3a**.

To address the challenge of detecting catechol aldehydes, especially within live cells, we introduce a novel approach using dual-reaction trigger FRET-based sensors. These sensors exploit both the aldehyde and catechol components of CAs, allowing for their selective detection amidst other aldehydes and catechols. By utilizing two reactions, involving diamine-phenyl-BODIPY **1a** with the aldehyde component to generate benzimidazole-BODIPY **2a**, and phenyl boronic acid-functionalized Rhodamine B **3a** with the catechol component to generate RhoB-boronic ester **4a**, our sensors produce distinct FRET signals for catechol aldehydes, enabling their selective identification within live cells in the presence of other aldehydes and catechols (**Figure 2**).

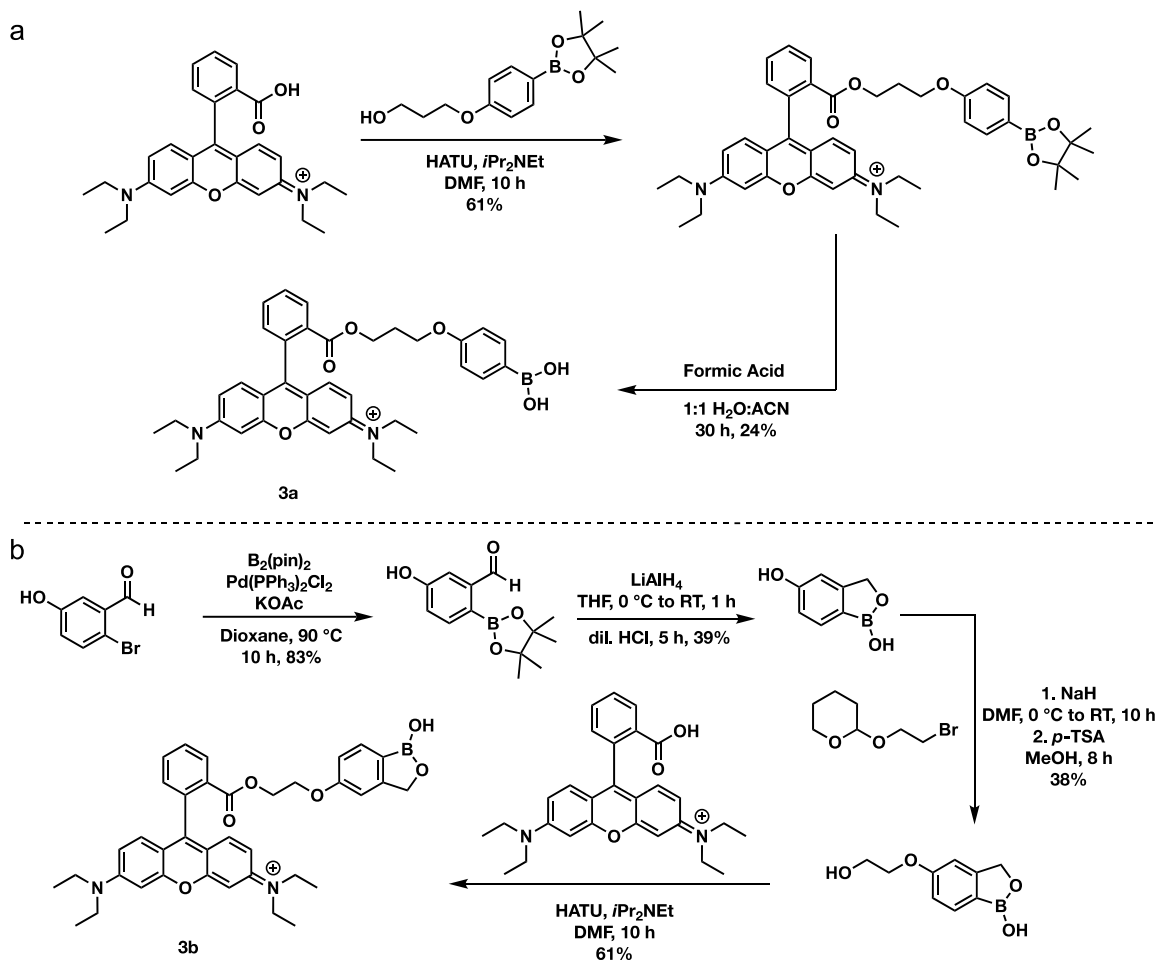
To accurately quantify catechol aldehyde levels, we employed Fluorescence Lifetime Imaging Microscopy combined with FRET (FLIM-FRET), providing nanosecond-scale fluorescence lifetime measurements.<sup>39-40</sup> The fluorescence lifetime of the donor decreases when its emission is quenched through a FRET interaction. FLIM-FRET offers robustness against various sources of interference, including spectral cross-talk, fluctuations in excitation intensity, inner filtering, photobleaching, direct acceptor excitation, and detector sensitivity,<sup>41</sup> making it suitable for live cells and tissues.<sup>42-43</sup> Its lower limit of detection allows for the identification of minute fractions of molecules engaged in FRET, enabling accurate measurements of aldehyde levels.<sup>41</sup> Our study successfully detected endogenous levels of catechol aldehydes within live cells, and notified changes in catechol aldehyde levels in response to enzyme activators and inhibitors. Furthermore, we demonstrated the application of our dual-reaction trigger FLIM-FRET system for identifying DOPEGAL specifically in the locus coeruleus (LC) of the brain in wild-type and diseased mice, indicating its potential for studying catechol aldehyde-related pathologies.

## Results and Discussion

### Development of FRET Probes for Catechol Aldehydes

In pursuit of our objectives, our laboratory has developed a probe utilizing 3,4-phenylenediamine linked to the BODIPY core, **1a**.<sup>44-45</sup> Probe **1a** exhibits notable chemoselectivity for aldehydes in the presence of other biological metabolites. Upon reacting with DOPAL, probe **1a** produced DOPAL-benzimidazole-BODIPY **2a**, resulting in a distinctive fluorescence activation at 507 nm. To selectively distinguish and identify catechol aldehydes from other reactive aldehydes, we devised a plan to leverage the distinctive catechol (1,2-dihydroxyphenyl) group of catechol aldehydes. We synthesized a phenylboronic acid-functionalized RhodamineB **3a** ( $\lambda_{ab}$  =546 nm) to serve as a FRET acceptor for the DOPAL-benzimidazole-BODIPY FRET donor **2a** ( $\lambda_{em}$  =507 nm), by the formation of boronate ester **4a** with the catechol group of **2a**.<sup>46</sup> To further enhance the reaction rate with the catechol component of catechol aldehydes and to obtain the best response profile while enhancing the stability of the boronate ester under physiological conditions, we synthesized heterocyclic benzoxaboroles-functionalized RhodamineB **3b** as a FRET acceptor.<sup>47</sup> RhodamineB was selected as the FRET acceptor due to its established efficacy in FRET with BODIPY and compatibility in live cells and living systems.<sup>48-49</sup>

Synthesis of probe **3a** began with coupling RhodamineB to commercially available boronate ester before subsequent pinacol deprotection (Scheme 1a, Supplementary Figure 1). Probe **3b** began with a Suzuki coupling of 2-Bromo-5-hydroxybenzaldehyde with  $B_2Pin_2$ , which was converted to benzoxaborole product using  $LiAlH_4$  before quenching in acidic conditions. Subsequent linker addition and coupling to RhodamineB yielded **3b** (Scheme 1b, Supplementary Figure 2).



**Scheme 1.** Synthesis of FRET Acceptors. **a)** Synthesis of **3a**. **b)** Synthesis of **3b**.

To assess the selectivity of these FRET pairs for catechol aldehydes, we initially incubated probe **1a** with various aldehydes, including acetaldehyde, propanal, butanal, valeraldehyde, octanal, and DOPAL, and recorded the absorbance and emission spectra of the corresponding benzimidazole products. A uniquely high absorbance and emission intensity were observed with DOPAL-benzimidazole-BODIPY **2a** compared to other aldehydes at the same concentrations, highlighting the role of catechol groups in enhancing the intensity of absorbance and emission (Figure 3a, Supplementary Figure 3). Interestingly, **2a** exhibited a higher quantum yield of 0.29 compared to **2b** with exhibited a quantum yield of 0.25 (Supplementary Figure 4). Next, phenylboronic acid-functionalized RhodamineB **3a** was added to DOPAL-benzimidazole-BODIPY **2a** at varying concentrations to determine its FRET efficiency. As expected, a dose-dependent increase in FRET efficiency was observed, with a maximum FRET efficiency of 97% at a 20 equiv. **3a** relative to **2a** (Figure 3b and Figure 3c). No FRET signals were observed with other aldehydes and catechols such as dopamine or norepinephrine due to the absence of both the aldehyde and catechol groups in the same structure. This selectivity towards catechol aldehydes stemmed from the chemoselective reaction between the 1,2-dihydroxyphenyl group of catechol aldehydes and the phenylboronic acid on the FRET acceptor, generating a boronate ester.<sup>46</sup>

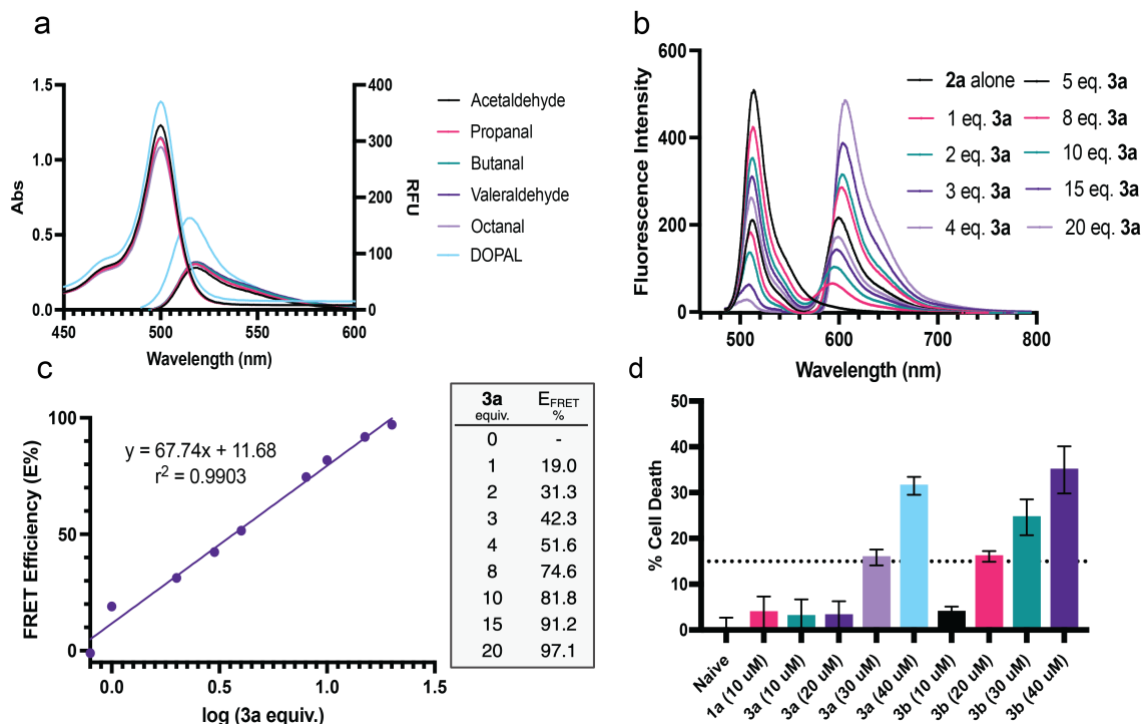


**Figure 3.** Fluorescent properties of probes **1a** and **3a** **a)** Excitation and emission of the products of the reaction of probe **1a** with varying aldehydes. RFU = relative fluorescent units. **b)** Emission of FRET donor **2a** with varying equivalence of FRET acceptor **3a**. **c)** Calculated FRET efficiencies tabulated and plotted against equiv. of **3a**. **d)** Cell death of U-87 MG cells incubated with probes **1a**, **3a**, and **3b**. All the experiments are performed in triplicate.

### Live Cell Compatibility and Selective Identification of Catechol Aldehydes by FLIM-FRET

To assess the operational efficacy of probes **1a**, **3a**, and **3b** within live cells, we incubated them with U-87 MG, a human glioblastoma cell line commonly utilized in brain research,<sup>50</sup> at various concentrations: **1a** (10  $\mu\text{M}$ ) and **3a** and **3b** (ranging from 10  $\mu\text{M}$  to 40  $\mu\text{M}$ ) for 2 hours, followed by flow cytometry analysis. The results unveiled over 95% cell viability with 10  $\mu\text{M}$  of **1a**, 20  $\mu\text{M}$  of **3a**, and 10  $\mu\text{M}$  of **3b**. However, concentrations exceeding 20  $\mu\text{M}$  of **3a** and 20-40  $\mu\text{M}$  of **3b** led to more than 15% cell death (Figure 3d, Supplementary Figure 5). Due to the high cell death observed with **3b**, we opted to proceed with utilizing 20  $\mu\text{M}$  of **3a** for live cell studies. Employing preformed DOPAL-benzimidazole-BODIPY **2a** and propanal-benzimidazole-BODIPY **2b**, we examined the capability of phenylboronic acid-functionalized RhodamineB **3a** to exhibit the FLIM-FRET signal within live cells. U-87 MG cells treated with **2a** (10  $\mu\text{M}$ ) for 2 hours, then were exposed to **3a** (20  $\mu\text{M}$ ) for 20 minutes, and the FLIM-FRET signal was measured using a Leica Stellaris 8 microscope (Figure 4).<sup>39-41</sup>

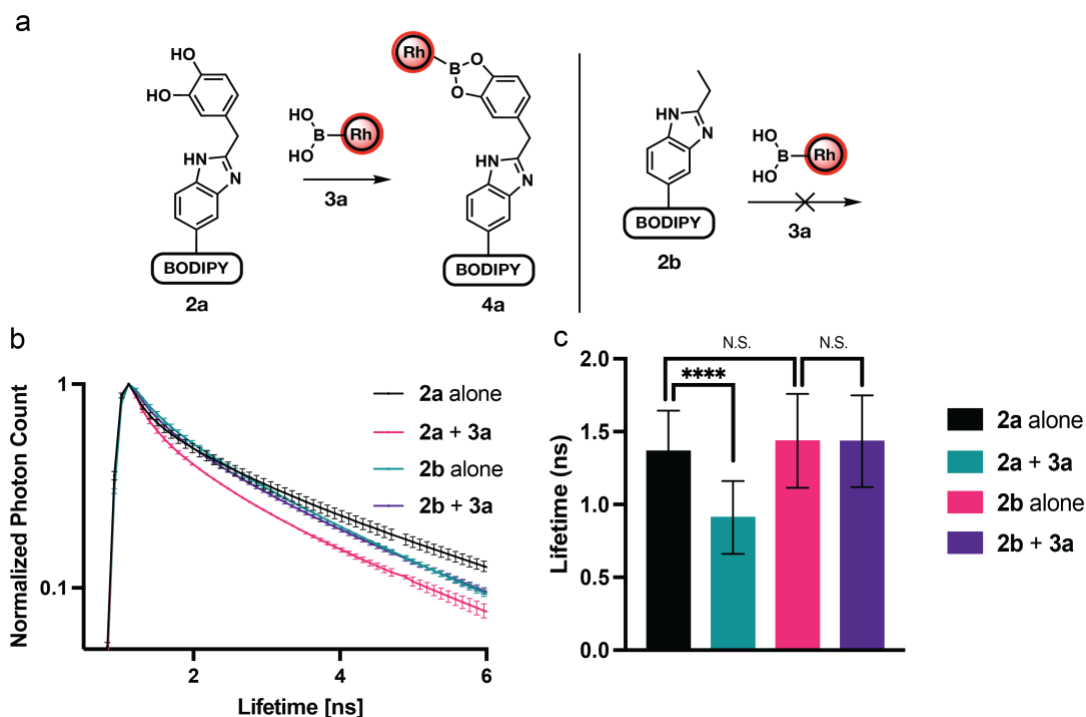


**Figure 4.** Selectivity of **2a** and **3a** FRET pair and resulting change in fluorescent lifetime  
**a)** Representation of FRET donor **2a** covalently interacting with FRET acceptor **3a** to give complex **4a** while **2b** is unable to form an analogous product. **b)** Lifetime decay curve of normalized photon counts of **2a** and **2b** alone and in the presence of **3a** in U-87 MG cells. No change in lifetime decay curve for **2b** in the presence of **3a**. All the experiments are performed in triplicate. **c)** Average fluorescent lifetime of **2a** and **2b** alone and in the presence of **3a** in U-87 MG cells. All the experiments are performed in triplicate. N.S. = not significant, \*\*\*\* =  $p < 0.0001$ .

The DOPAL-benzimidazole-BODIPY **2a** had an average lifetime of 1.364 ns while the propanal-benzimidazole-BODIPY **2b** had an average lifetime of 1.436 ns. When probe **3a** was introduced to cells, **2a** showed a reduction in average fluorescent lifetime to 0.911 ns, while **2b** had no noticeable change in the fluorescence lifetime with an average of 1.434 ns (**Figure 4**, Supplementary Figure 6). Decrease in fluorescence lifetime was observed exclusively with catechol aldehydes (DOPAL), with a FRET efficiency ( $E$ ) of 34.4%, thus highlighting its potential in selectively detecting catechol aldehydes within live cellular environments. This selectivity towards catechol aldehydes stemmed from the chemoselective reaction between the 1,2-dihydroxyphenyl group of catechol aldehydes and the phenylboronic acid on the FRET acceptor, generating a boronate ester inside live cells.

### Live Cell Imaging and Monitoring of Exogenous Catechol Aldehyde Levels in Preclinically Relevant Disease Models

To evaluate the efficacy of our dual-reaction trigger FLIM-FRET system in detecting natural DOPAL production during metabolic processes within live cells, we treated U-87 MG cells with dopamine (DA) (for DOPAL production), alone and in combination with dexamethasone (Dexa) (an MAO activator),<sup>51</sup> diadzin (DDZ),<sup>52</sup> and benomyl (Ben)<sup>53</sup>

(ALDH2 and ALDH inhibitors, respectively), either individually or in combination for 15 minutes. Subsequently, the cells were co-treated with 10  $\mu$ M of probe **1a** for 2 hours, before treatment with 20  $\mu$ M of FRET acceptor **3a** for 15 minutes (**Figure 5a**). Observation of the cells using a Leica microscope revealed a significant decrease in the fluorescence lifetime of the donor complex **2a** generated by the reaction of **1a** with DA metabolite, DOPAL, followed by the FRET complex formation with **3a** (0.765 ns, 35.7%) (**Figure 5a**, Supplementary Figure 7). Addition of MAO activator, Dexa resulted in further lowering of fluorescence lifetime (0.650 ns, 45.4%) due to overproduction of DOPAL (**Figure 5a**, Supplementary Figure 7). The addition of DDZ (0.672 ns, 43.1%), and Ben (0.712 ns, 39.7%) further lowered the fluorescence lifetime of **2a**. The change in lifetimes can be visualized by phasor plots with the formation of a new cluster of lifetimes (**Figure 5c**, Supplementary Figure 7). This decrease is primarily attributed to the increased DOPAL production from dopamine and its accumulation due to the inhibition of DOPAL conversion to 3,4-dihydroxyphenylacetic acid (DOPAC).<sup>4-5</sup>, revealing that the combined treatment of DA/Dexa/DDZ/Ben yielded a significant lowering in the fluorescence lifetime of the **2a** to 0.564 ns corresponding to enhanced cellular concentration of DOPAL (**Figure 5a**, Supplementary Figure 7). The results clearly demonstrated higher concentrations of DOPAL in the presence of both the MAO activator and ALDH inhibitors.

To investigate whether the acceleration of endogenous norepinephrine (NE) metabolism and DOPEGAL production<sup>5,38</sup> would yield similar effects, we incubated live U-87 MG cells with NE, followed by MAO activator and/or ALDH inhibitors along with the donor probe **1a** followed by acceptor probe **3a** (**Figure 5d-f**, Supplementary Figure 8). Similar to observations with dopamine metabolism, a decrease in the fluorescence lifetime of the donor **1a** with NE (0.723 ns, 34.3%) was observed in the presence of Dexa (0.597 ns, 45.8%), DDZ (0.632 ns, 42.6%), or Ben (0.666 ns, 39.6%), with a much larger decrease in the donor lifetime (0.541 ns, 50.5%) was observed in cells treated with all drugs (Dexa/DDZ/Ben) in combination indicating the metabolism of NE to DOPEGAL and the formation of FRET by the reaction of DOPEGAL with probe **1a**, followed by quenching through complex formation with FRET acceptor **3a** inside live cells (**Figure 5d-f**, Supplementary Figure 8). These findings underscore the sensitivity of our dual-reaction trigger FLIM-FRET system in monitoring disease states resulting from alterations in catechol aldehyde levels, indicating its potential utility across diverse pathogenic conditions.

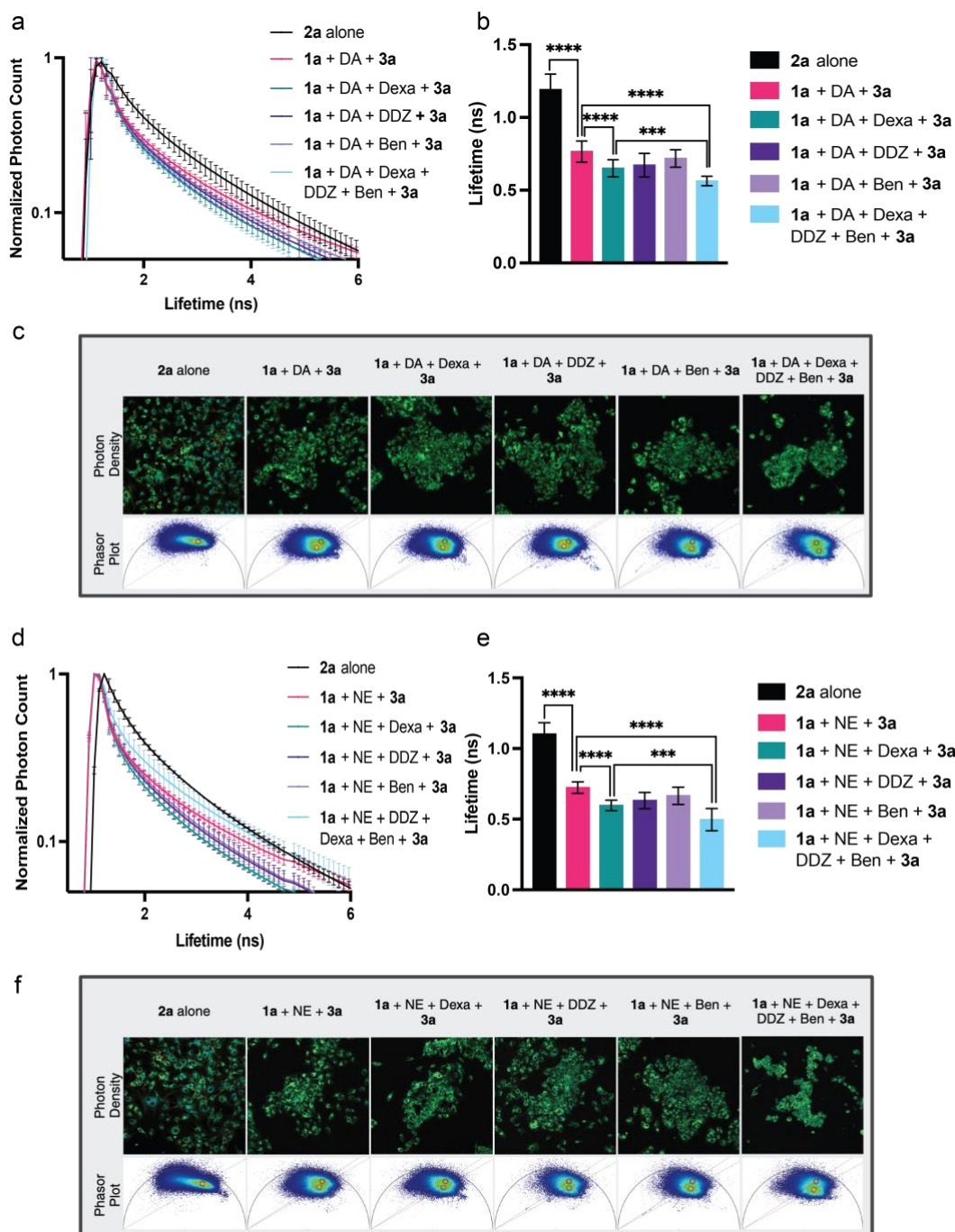


**Figure 5.** Live cell FLIM-FRET analysis of U-87 MG cells dosed with exogenous dopamine and norepinephrine **a)** Lifetime decay curve of the normalized photon count for **2a** in the presence of **3a** in U-87 MG cells treated with exogenous dopamine (DA), Dexa, DDZ, and Ben individually and in combination. All the experiments were performed in triplicate. **b)** Average fluorescent lifetime of **2a** in the presence of **3a** in U-87 MG cells in the presence of exogenous dopamine (DA), Dexa, DDZ, and Ben individually and in combination. All the experiments were performed in triplicate. **c)** Representative image of photon density of U-87 MG cells and corresponding phasor plots. **d)** Lifetime decay curve of the normalized photon count for a donor complex between **1a** and DOPEGAL in the

presence of **3a** in U-87 MG cells treated with exogenous norepinephrine (NE), Dexa, DDZ, and Ben individually and in combination. All the experiments were performed in triplicate. **e)** Average fluorescent lifetime of a donor complex between **1a** and DOPEGAL in the presence of **3a** in U-87 MG cells in the presence of exogenous dopamine (DA), Dexa, DDZ, and Ben individually and in combination. All the experiments were performed in triplicate. **f)** Representative image of photon density of U-87 MG cells and corresponding phasor plots. \*\* =  $p < 0.01$ , \*\*\* =  $p < 0.001$ , \*\*\*\* =  $p < 0.0001$ .

### Live Cell Imaging and Monitoring of Endogenous DOPAL and DOPEGAL Levels in Parkinsons Disease model

Building upon these promising results, we proceeded to detect and quantify the endogenous levels of catechol aldehydes, including both DOPAL and DOPEGAL, within live cells. U-87 MG cells were treated with Dexa, DDZ, and Ben, either individually or in combination, followed by treatment with 10  $\mu\text{M}$  of probe **1a** for 2 hours, then 20  $\mu\text{M}$  of FRET acceptor **3a** for 15 minutes. A decrease in the fluorescence lifetime of the donor **2a** (0.782 ns, 25.2%) was observed in the presence of Dexa (0.691 ns, 33.8%), DDZ (0.663 ns, 36.5%), or Ben (0.681 ns, 34.8%), with a much larger decrease in the donor lifetime (0.601 ns, 44.9%) was observed in cells treated with all drugs (Dexa/DDz/Ben) in combination (**Figure 6**, Supplementary Figure 9). These results affirm the high sensitivity and rapid kinetics of our FRET probes **1a** and **3a**, qualifying them for the identification of natural aldehyde production in both diseased and non-diseased cellular states.

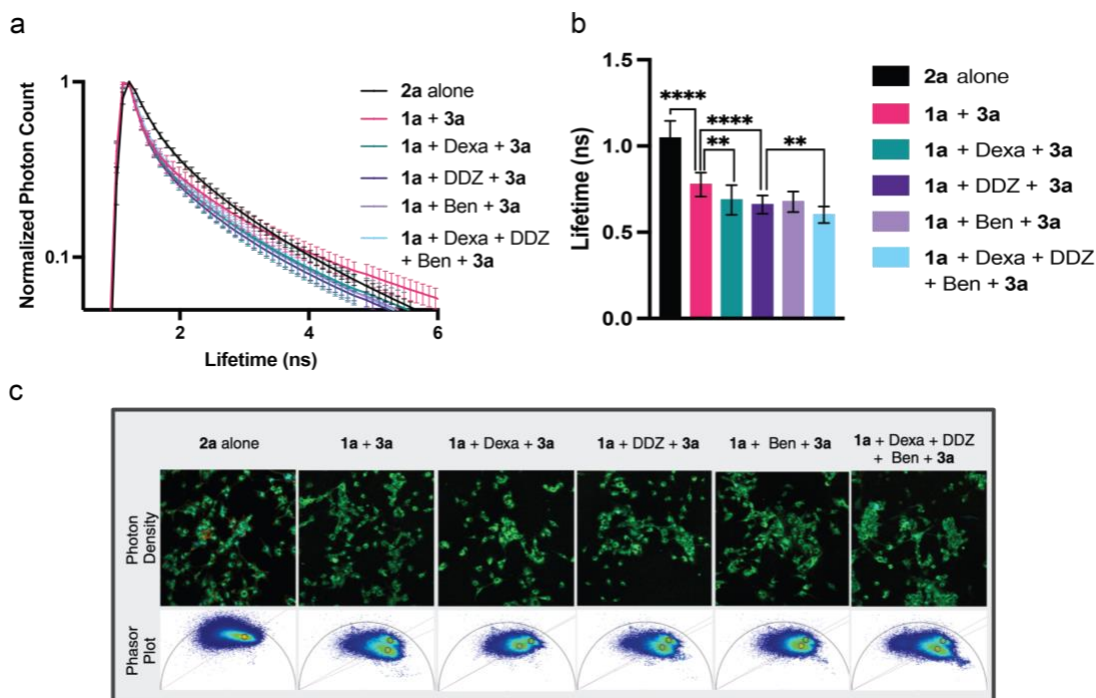


**Figure 6.** Live cell FLIM-FRET analysis of U-87 MG cells for endogenous DOPAL and DOPEGAL detection. **a)** Lifetime decay curve of the normalized photon count for complexes between **1a** and DOPAL and DOPEGAL in the presence of **3a** in U-87 MG cells treated with MAO activator (Dexa) and ALDH inhibitors (DDZ and Ben) individually and in combination. All the experiments are performed in triplicate. **b)** Average fluorescent lifetime of complexes between **1a** and DOPAL and DOPEGAL in the presence of **3a** in U-

87 MG cells treated with MAO activator (Dexa) and ALDH inhibitors (DDZ, and Ben) individually and in combination. All the experiments are performed in triplicate. **c)** Representative image of photon density of U-87 MG cells and corresponding phasor plots. ns = not significant, \*\* =  $p < 0.01$ , \*\*\* =  $p < 0.001$ , \*\*\*\* =  $p < 0.0001$ .

### Detection and Quantification of DOPEGAL *in vivo*

Encouraged by these outcomes, we applied our system to identify DOPEGAL in the locus coeruleus (LC) of mice, the primary source NE in the brain.<sup>54-55</sup> To verify the specificity of our probes to identify and quantify NE metabolic products in living systems, we compared signal in wild-type (WT) and dopamine  $\beta$ -hydroxylase knockout (DBH  $-/-$ ) mice, which lack NE production and thus cannot generate DOPEGAL.<sup>56</sup> After sacrifice and isolation of the intact brain, it was incubated with probe **1a** for 2 hours, followed by probe **3a** for 15 minutes, followed by cryosection to isolate the LC and subsequent imaging (**Figure 7a**, Supplementary Figure 10). As expected, a significantly lower fluorescence lifetime of the FRET donor **1a** (1.015 ns average from 3 images per slice of tissue, 2 tissue slices per mouse with 2 mice) was observed in the LC from WT mice compared to that from DBH knockout mice (1.777 ns average from 3 images per slice of tissue, 2 tissue slices per mouse with 2 mice). Additionally, FLIM-FRET pixel intensity allows for the analysis of spatiotemporal information regarding NE concentration (**Figure 7b**, Supplementary Figure 10). These results confirm that our probes can specifically detect NE metabolites such as DOPEGAL in native murine brain tissue. Given that DOPEGAL in the LC contributes to Tau aggregation and propagation to the forebrain, our probes have the potential to serve as an early warning signal for brainstem Tau pathology, offering a valuable diagnostic tool for the onset of Alzheimer's disease.

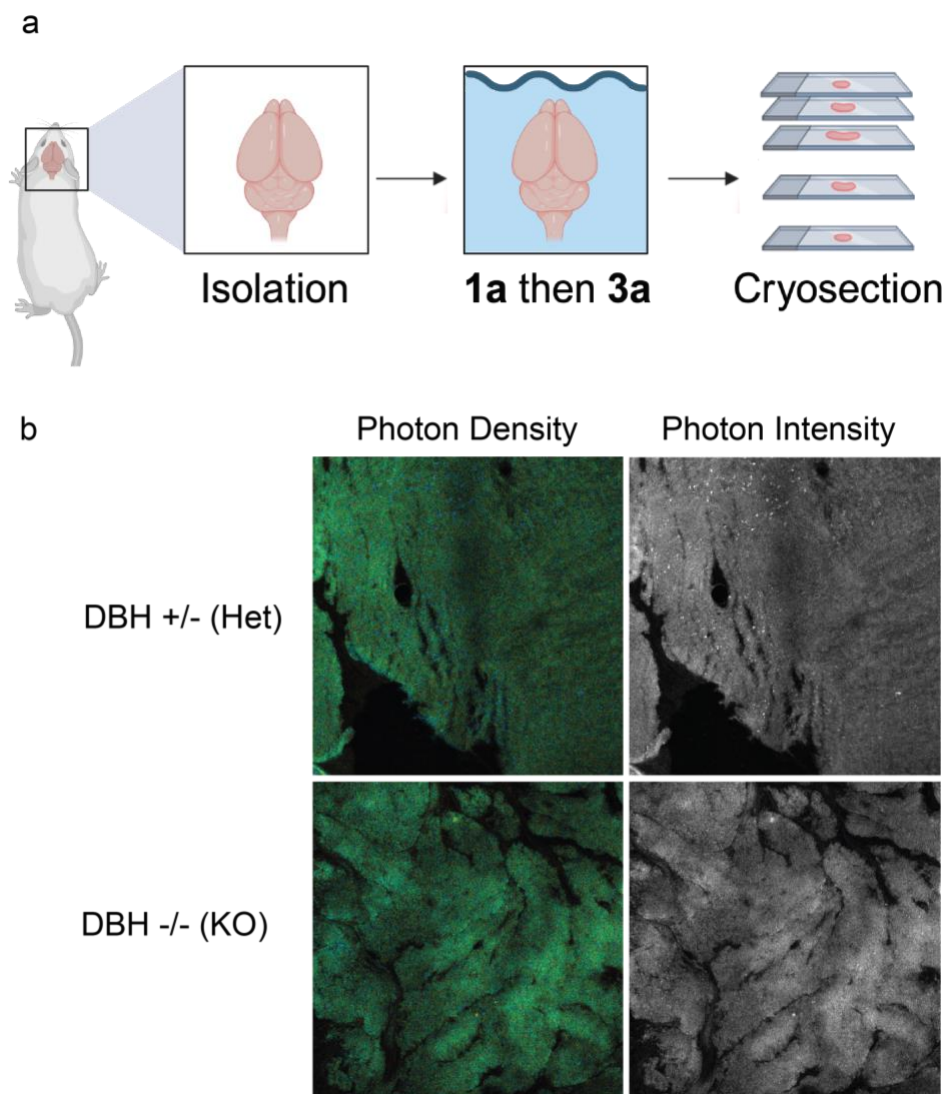


**Figure 7.** Tissue imaging of WT mice and dopamine  $\beta$ -hydroxylase knockout mice with probe **1a** and **3a**. **a)** Schematic of tissue imaging protocol in WT mice and DBH knockout (DBH  $-/-$ ) mice. **b)** FLIM photon density and photon intensity of DBH +/- (Het) and DBH  $-/-$  (KO) mice brain LC tissue. Light blue pixels in photon density represent lower average fluorescent lifetime which are alternatively visualized as white hot spots in photon intensity images.

### Conclusion

In this research endeavor, we have successfully developed a FRET donor-acceptor pair coupled with FLIM, enabling the selective detection of catechol aldehydes within living systems. This method operates as a dual-reaction trigger FLIM-FRET system, necessitating the presence of both an aldehyde group and a catechol group on the same molecule for efficient FRET signaling, thus demonstrating high selectivity for detecting catechol aldehydes specifically in the presence of other aldehydes and catechols in living systems. The reaction between 3,4-diamino-BODIPY and catechol aldehyde, DOPAL,

yields DOPAL-benzimidazole-BODIPY (**2a**), leading to a remarkable 34-fold increase in fluorescence. Conversely, the reaction of the catechol group of DOPAL-benzimidazole-BODIPY with phenylboronic acid-functionalized RhodamineB forms a boronic ester, facilitating efficient FRET signaling between the donor benzimidazole-BODIPY and acceptor RhodamineB. The lower fluorescence lifetime of the donor in the presence of the acceptor indicates the high FRET efficiency of our system, rendering it ideal for detecting and quantifying concentrations of catechol aldehydes in living systems using FLIM-FRET, without susceptibility to interference from fluctuations in excitation intensity, inner filtering, photobleaching, spectral cross-talk, and direct acceptor excitation. We have demonstrated the ability of dual-reaction trigger FLIM-FRET system to detect and quantify both exogenous and endogenous levels of catechol aldehydes, DOPAL, and/or DOPEGAL in live cells, further validated by their capability to detect aldehyde fluctuations in disease models. This sensitivity and real-time measurement capability position them as promising candidates for exploring the role of catechol aldehydes in various cellular processes. Notably, we applied these probes to detect DOPEGAL in the locus coeruleus (LC) of wild-type (WT) mouse brains and compared them with DBH knockout (DBH  $-/-$ ) mice lacking NE production, underscoring their value in biomedical research. Collectively, our probes offer a valuable tool for investigating catechol aldehyde dynamics in biological systems, devoid of interference from other biological metabolites. This capability facilitates deeper exploration of catechol aldehyde processes, fostering research into catechol aldehyde-related pathogenesis. This work establishes a foundation for future investigations exploring potential applications in developing diagnostic tools providing early warning signals for neurological, cardiovascular and metabolic disorders.

## References

1. Kopin, I. J. Storage and metabolism of catecholamines: the role of monoamine oxidase. *Pharmacological Reviews*. **1964**, *16*, 179-191.
2. Collins, G. G.; Sandler, M.; Williams, E. D.; Youdim, M. B. Multiple forms of human brain mitochondrial monoamine oxidase. *Nature*, **1970**, *225*, 817-820.
3. Goldstein, D. S.; Castillo, G.; Sullivan, P.; Sharabi, Y. Differential susceptibilities of catecholamines to metabolism by monoamine oxidases. *J. Pharmacol. Exp. Ther.* **2021**, *379*, 253-259.
4. Blaschko, H. Metabolism and storage of biogenic amines. *Experientia* **1957**, *13*, 9–13.
5. Goldstein, D. S. The Catecholaldehyde Hypothesis for the pathogenesis of catecholaminergic neurodegeneration: what we know and what we do not know. *Int. J. Mol. Sci.* **2021**, *22*, 5999-6018.
6. Masato, A.; Plotegher, N.; Boassa, D.; Bubacco, L. Impaired dopamine metabolism in Parkinson's disease pathogenesis. *Mol. Neurodegener.* **2019**, *14*, 35-56.
7. MacKerell, A. D., Jr.; Pietruszko, R. Chemical modification of human aldehyde dehydrogenase by physiological substrate. *Biochim. Biophys. Acta.* **1987**, *911*, 306-317.
8. Crawford, R. A.; Bowman, K. R.; Cagle, B. S.; Doorn, J. A. In vitro inhibition of glutathione-S-transferase by dopamine and its metabolites, 3,4-dihydroxyphenylacetaldehyde and 3,4-dihydroxyphenylacetic acid. *NeuroToxicology*

2021, 86, 85-93.

9. Mexas, L. M.; Florang, V. R.; Doorn, J. A. Inhibition and covalent modification of tyrosine hydroxylase by 3,4-dihydroxyphenylacetaldehyde, a toxic dopamine metabolite. *NeuroToxicology* **2011**, *32*, 471-477.

10. Vermeer, L. M.; Florang, V. R.; Doorn, J. A. Catechol and aldehyde moieties of 3,4-dihydroxyphenylacetaldehyde contribute to tyrosine hydroxylase inhibition and neurotoxicity. *Brain Res.* **2012**, *1474*, 100-109.

11. Crawford, R. A.; Gilardoni, E.; Monroe, T. B.; Regazzoni, L.; Anderson, E. J.; Doorn, J. A. Characterization of catecholaldehyde adducts with carnosine and L-Cysteine reveals their potential as biomarkers of catecholaminergic stress. *Chem. Res. Toxicol.* **2021**, *34*, 2184-2193.

12. Rees, J. N.; Florang, V. R.; Eckert, L. L.; Doorn, J. A. Protein reactivity of 3,4-dihydroxyphenylacetaldehyde, a toxic dopamine metabolite, is dependent on both the aldehyde and the catechol. *Chem. Res. Toxicol.* **2009**, *22*, 1256-1263.

13. Anderson, D. G.; Florang, V. R.; Schamp, J. H.; Buettner, G. R.; Doorn, J. A. Antioxidant-mediated modulation of protein reactivity for 3,4-dihydroxyphenylacetaldehyde, a toxic dopamine metabolite. *Chem. Res. Toxicol.* **2016**, *29*, 1098-1107.

14. Jinsmaa, Y.; Florang, V. R.; Rees, J. N.; Mexas, L. M. Eckert, L. L.; Allen, E. M. G.; Anderson, D. G.; Doorn, J. A. Dopamine-derived biological reactive intermediates and protein modifications: Implications for Parkinson's disease. *Chem. Biol. Interact.* **2011**, *192*, 118-121.

15. Anderson, D. G.; Mariappan, S. V.; Buettner, G. R.; Doorn, J. A. Oxidation of 3,4-dihydroxyphenylacetaldehyde, a toxic dopaminergic metabolite, to a semiquinone radical and an ortho-quinone. *J. Biol. Chem.* **2011**, *286*, 26978-26986.

16. Wanner, M. J.; Zuidinga, E.; Tromp, D. S.; Vilím, J.; Jørgensen, S. I.; van Maarseveen, J. H. Synthetic evidence of the amadori-type alkylation of biogenic amines by the neurotoxic metabolite DOPEGAL. *J. Org. Chem.* **2020**, *85*, 1202-1207.

17. Follmer, C.; Coelho-Cerqueira, E.; Yatabe-Franco, D. Y.; Araujo, G. D.; Pinheiro, A. S.; Domont, G. B.; Eliezer, D. Oligomerization and membrane-binding properties of covalent adducts formed by the interaction of  $\alpha$ -synuclein with the toxic dopamine metabolite 3,4-Dihydroxyphenylacetaldehyde (DOPAL). *J. Biol. Chem.* **2015**, *290*, 27660-27679.

18. Jinsmaa, Y.; Sullivan, P.; Sharabi, Y.; Goldstein, D. S. DOPAL is transmissible to and oligomerizes alpha-synuclein in human glial cells. *Auton. Neurosci.* **2016**, *194*, 46-51.

19. Kang, S. S.; Ahn, E. H.; Zhang, Z.; Liu, X.; Manfredsson, F. P.; Sandoval, I. M.; Dhakal, S.; Iuvone, P. M.; Cao, X.; Ye, K.  $\alpha$ -Synuclein stimulation of monoamine oxidase-B and

legumain protease mediates the pathology of Parkinson's disease. *EMBO J.* **2018**, *37*, e98878.

20. Kang, S. S.; Liu, X.; Ahn, E. H.; Xiang, J.; Manfredsson, F. P.; Yang, X.; Luo, H. R.; Liles, L. C.; Weinschenker, D.; Ye, K. Norepinephrine metabolite DOPEGAL activates AEP and pathological Tau aggregation in locus coeruleus. *J. Clin. Invest.* **2020**, *130*, 422–437.

21. Jenner, P. Oxidative stress in Parkinson's disease. *Ann. Neurol.* **2003**, *53*, S26–S36.

22. Nelson, M.-A. M.; Efield, J. T.; Kew, K. A.; Katunga, L. A.; Monroe, T. B.; Doorn, J. A.; Beatty, C. N.; Shi, Q.; Akhter, S. A.; Alwair, H.; Robidoux, J.; Anderson, E. J. Enhanced Catecholamine Flux and Impaired Carbonyl Metabolism Disrupt Cardiac Mitochondrial Oxidative Phosphorylation in Diabetes Patients. *Antioxid. Redox Signal.* **2021**, *35*, 235–251.

23. Nelson, M.-A. M.; Builta, Z. J.; Monroe, T. B.; Doorn, J. A.; Anderson, E. J. Biochemical characterization of the catecholaldehyde reactivity of L-carnosine and its therapeutic potential in human myocardium. *Amino Acids* **2019**, *51*, 97–102.

24. Bianchi, P.; Kunduzova, O.; Masini, E.; Cambon, C.; Bani, D.; Raimondi, L.; Seguelas, M.-H.; Nistri, S.; Colucci, W.; Leducq, N.; Parini, A. Oxidative stress by monoamine oxidase mediates receptor-independent cardiomyocyte apoptosis by serotonin and postischemic myocardial injury. *Circulation* **2005**, *112*, 3297–3305.

25. Kaludercic, N.; Takimoto, N.; Feng, N.; Lai, E. W.; Bedja, D.; Chen, K.; Gabrielson, K. L.; Blakely, R. D.; Shih, J. C.; Pacak, K.; Kass, D. A.; Di Lisa, F.; Paolocci, N. Monoamine oxidase A-mediated enhanced catabolism of norepinephrine contributes to adverse remodeling and pump failure in hearts with pressure overload. *Circ. Res.* **2009**, *106*, 193–202.

26. Nováková, D.; Kudláček, K.; Novotný, J.; Nesměrák, K. Improvement of conditions for the determination of neurotransmitters in rat brain tissue by HPLC with fluorimetric detection. *Monatsh. Chem.* **2022**, *153*, 753–758.

27. Olesti, E.; Rodriguez-Morato, J.; Gomez-Gomez, A.; Ramaekers, J.G.; de la Torre, R.; Pozo, O.J. Quantification of endogenous neurotransmitters and related compounds by liquid chromatography coupled to tandem mass spectrometry. *Talanta* **2019**, *192*, 93–102.

28. Chefer, V. I.; Thompson, A. C.; Zapata, A.; Shippenberg, T. S. Overview of brain microdialysis. *Curr. Protoc. Neurosci.* **2009**, *47*, 7.1.1–7.1.28.

29. Roychoudhury, A.; Francis, K. A.; Patel, J.; Jha, S. K.; Basu, S. A decoupler-free simple paper microchip capillary electrophoresis device for simultaneous detection of dopamine, epinephrine and serotonin. *RSC Adv.* **2020**, *10*, 25487–25495.

30. Luo, Y.; Kim, E. H.; Flask, C. A.; Clark, H. A. Nanosensors for the Chemical Imaging of Acetylcholine Using Magnetic Resonance Imaging. *ACS Nano* **2018**, *12*, 5761–5773.

31. Binnie, C.; Prior, P. Electroencephalography. *J. Neurol. Neurosurg. Psychiatry* **1994**,

57, 1308–1319.

32. Chauhan, N.; Soni, S.; Agrawal, P.; Balhara, Y. P. S.; Jain, U. Recent advancement in nanosensors for neurotransmitters detection: Present and future perspective. *Process Biochem.* **2020**, *91*, 241–259.

33. Finkel, T.; Holbrook, N. J. Oxidants, oxidative stress and the biology of ageing. *Nature* **2000**, *408*, 239–247.

34. Lin, M. T.; Beal, M. F. Mitochondrial dysfunction and oxidative stress in neurodegenerative diseases. *Nature* **2006**, *443*, 787–795.

35. Werner-Allen, J. W.; DuMond, J. F.; Levine, R. L.; Bax A. Toxic dopamine metabolite DOPAL forms an unexpected dicatechol pyrrole adduct with lysines of alpha-synuclein. *Angew. Chem. Int. Ed.* **2016**, *55*, 7374-7378.

36. Werner-Allen, J. W.; Levine, R. L.; Bax A. Superoxide is the critical driver of DOPAL autoxidation, lysyl adduct formation, and crosslinking of alpha-synuclein. *Biochem. Biophys. Res. Commun.* **2016**, *487*, 281-286.

37. Werner-Allen, J. W.; Monti, S.; DuMond, J. F.; Levine, R. L.; Bax, A. Isoindole linkages provide a pathway for DOPAL-mediated cross-linking of alpha-synuclein. *Biochemistry* **2018**, *57*, 1462-1474.

38. Riederer, P.; Berg, D.; Casadei, N.; Cheng, F.; Classen, J.; Dresel, C.; Jost, W.; Krüger, R.; Müller, T.; Reichmann, H.; Rieß, O.; Storch, A.; Strobel, S.; van Eimeren, T.; Völker, H. U.; Winkler, J.; Winklhofer, K. F.; Wüllner, U.; Zunke, F.; Monoranu, C. M.  $\alpha$ -Synuclein in Parkinson's disease: causal or bystander? *J. Neural. Transm.* **2019** *126*, 815-840.

39. Bajar, B. T.; Wang, E. S.; Zhang, S.; Lin, M. Z.; Chu, J. A guide to fluorescent protein FRET pairs. *Sensors* **2016**, *16*, 1488-1511.

40. Becker, W. Fluorescence lifetime imaging--Techniques and applications. *J. Microsc.* **2012**, *247*, 119–136.

41. Pietraszewska-Bogiel, A.; Gadella, T. W. FRET microscopy: from principle to routine technology in cell biology. *J. Microsc.* **2011**, *241*, 111–118.

42. Day, R. N.; Davidson, M. W. Fluorescent proteins for FRET microscopy: Monitoring protein interactions in living cells. *Bioessays* **2012**, *34*, 341–350.

43. McGinty, J.; Stuckey, D. W.; Soloviev, V. Y.; Laine, R.; Wylezinska-Arridge, M.; Wells, D. J.; Arridge, S. R.; French, P. M.; Hajnal, J. V.; Sardini, A. In vivo fluorescence lifetime tomography of a FRET probe expressed in mouse. *Biomed. Opt. Express* **2011**, *2*, 1907–1917.

44. Wills, R.; Farhi J.; Czabala, P.; Shahin, S.; Spangle, J. M.; Raj, M. Chemical sensors for imaging total cellular aliphatic aldehydes in live cells. *Chem. Sci.* **2023**, *14*, 8305-8314.
45. Wills, R.; Shirke, R.; Hrcir, H.; Talbott, J. M.; Sad, K.; Spangle, J. M.; Gracz, A. D.; Raj, M. Tunable fluorescent probes for detecting aldehydes in living systems. *Chem. Sci.* **2024**, *15*, 4673-4769.
46. Suzuki, Y.; Kusuyama, D.; Sugaya, T.; Iwatsuki, S.; Inamo, M.; Takagi, H. D.; Ishihara, K. Reactivity of boronic acids toward catechols in aqueous solution. *J. Org. Chem.* **2020**, *85*, 5255-5264.
47. Brooks, W. L. A.; Deng, C. C.; Sumerlin, B. S. Structure–reactivity relationships in boronic acid–diol complexation. *ACS Omega* **2018**, *3*, 17863-17870.
48. Ulrich, G.; Ziesel, R.; Harriman, A. The chemistry of fluorescent BODIPY dyes: versatility unsurpassed. *Angew. Chem. Int. Ed.* **2008**, *47*, 1184–1201.
49. Boens, N.; Verbelen, B.; Dehaen, W. Postfunctionalization of the BODIPY core: synthesis and spectroscopy. *Eur. J. Org. Chem.* **2015**, *2015*, 6577–6595.
50. Allen, M.; Bjerke, M.; Edlund, H.; Nelander, S.; Westermark, B. Origin of the U87MG glioma cell line: Good news and bad news. *Sci. Transl. Med.* **2016**, *8*, 354re3.
51. Veals, J. W.; Korduba, C. A.; Symchowicz, S. Effect of dexamethasone on monoamine oxidase inhibition by iproniazid in rat brain *Eur. J. Pharmacol.* **1977**, *41*, 291-299.
52. Keung, W.-M.; Vallee, B. L. Diadzin: a potent, selective inhibitor of human mitochondrial aldehyde dehydrogenase. *Proc. Natl. Acad. Sci.* **1993**, *90*, 1247-1251.
53. Casida, J. E.; Ford, B.; Jinsmaa, Y.; Sullivan, P.; Cooney, A.; Goldstein, D. S. Benomyl, aldehyde dehydrogenase, DOPAL, and the catecholaldehyde hypothesis for the pathogenesis of Parkinson's disease. *Chem. Res. Toxicol.* **2014**, *27*, 1359–1361.
54. Kang, S. S.; Meng, L.; Zhang, X.; Wu, Z.; Mancieri, A.; Xie, B.; Weinshenker, D.; Peng, J.; Zhang, Z.; Ye, K. Tau modification by the norepinephrine metabolite DOPEGAL stimulates its pathology and propagation. *Nat. Struct. Mol. Biol.* **2022**, *29*, 292-305.
55. Kang, S. S.; Ahn, E. H.; Ye, K. Delta-secretase cleavage of Tau mediates its pathology and propagation in Alzheimer's disease. *Exp. Mol. Med.* **2020**, *52*, 1275-1287.
56. Levin, E. Y.; Levenberg, B.; Kaufman, S. The enzymatic conversion of 3,4-dihydroxyphenylethylamine to norepinephrine. *J. Biol. Chem.* **1960**, *235*, 2080-2086.

### Corresponding author

\*monika.raj@emory.edu

### Author contributions

R. W. and M. R. conceived the project. R. S. optimized synthetic routes for synthesis of probes. J. M. T. and R. W. conducted all cell experiments. J. M. T. and L. H. conducted mice tissue imaging. All authors have given approval to the final version of the manuscript.

### **Conflicts of interest**

There are no other conflicts to declare.

### **Acknowledgements**

This research was supported by NIH (No. 1R35GM133719-01) and NSF (Grant No. CHE-1752654 and CHE-2108774) to M. R. and NIH/NIA grant AG079199 to D.W. This work was supported by the Emory University Emory Integrated Cellular Imaging Core Facility (RRID:SCR\_023534). All graphs were produced in Prism and all the images are created with [biorender.com](https://biorender.com). All mouse experiments were conducted in accordance with protocols approved by the Institutional Animal Care and Use Committee (IACUC) of Emory University School of Medicine (EUCM).

### **Data availability**

The data supporting this article have been uploaded as part of the ESI.